Article:
Neal, J.S., Milosevic, M.V., Bending, S.J. et al. (2007) Competing symmetries and broken bonds in superconducting vortex-antivortex molecular crystals. Physical Review Letters, 99 (127001). ISSN: 1079-7114

https://doi.org/10.1103/PhysRevLett.99.127001

Published paper
Neal, J.S., Milosevic, M.V., Bending, S.J., Potenza, A., Emeterio, L.S. and Marrows, C.H. (2007), *Competing symmetries and broken bonds in superconducting vortex-antivortex molecular crystals,* Physical Review Letters, Volume 99 (127001).

Competing symmetries and broken bonds in superconducting vortex-antivortex "molecular crystals"

J. S. Neal, M. V. Milošević,* and S. J. Bending†
Department of Physics, University of Bath, Claverton Down, Bath BA2 7AY, UK

A. Potenza,‡ L. San Emeterio, and C. H. Marrows
School of Physics and Astronomy, University of Leeds, Leeds LS2 9JT, UK
(Dated: July 17, 2007)

Hall probe microscopy has been used to image vortex-antivortex "molecules" induced in superconducting Pb films by the stray fields from square arrays of magnetic dots. We have *directly* observed spontaneous vortex-antivortex pairs and studied how they interact with added "free" (anti)fluxons in an applied magnetic field. We observe a variety of phenomena arising from competing symmetries which either drive added antivortices to *join antivortex shells* around dots or stabilize the translationally symmetric antivortex lattice *between* the dots. Added vortices annihilate antivortex shells, leading first to a stable *'nulling state'* with no free fluxons and then, at high densities, to *vortex shells* around the dots stabilized by the asymmetric *anti-pinning* potential. Our experimental findings are in good agreement with Ginzburg-Landau calculations.

PACS numbers: 74.78.Na, 74.25.Ha, 74.20.De.

Two-dimensional ordering and crystallization of particles on structured substrates has attracted considerable attention in the past decade. For example, the rich crystalline states of colloidal particles have been examined both theoretically and experimentally [1], as well as the ordering of atoms on corrugated surfaces [2] and vortices in superconductors with periodic pinning arrays [3]. In such cases particles are grouped at substrate potential minima, and each of these *groups* can act as a single particle with internal degrees of rotational freedom, forming states that have additional long-range translational order. The existence of these competing symmetries gives rise to particularly subtle phenomena and leads to ordered states which are analogous to "molecular crystals".

The question of crystallization becomes particularly interesting when single species molecules are replaced by ionic ones containing positive and negative counterparts. Recently, colloidal crystals of oppositely charged particles have been experimentally realized [4]. Surprisingly, it was found that the stoichiometry of such crystals is not dictated by charge neutrality, allowing the formation of a diverse range of binary structures, which gradually melted upon application of an electric field. Analogous "ionic" structures can be found in superconductors; specifically in superconducting films deposited on spatial arrays of magnets. Each magnet may generate one or more spontaneous vortex-antivortex (V-AV) pairs in the superconducting film. These either remain associated with individual magnets as V-AV "molecules" [5] in dilute arrays, or organize themselves into an "ionic" crystal in dense arrays [6]. To date there has been no experimental verification of such spontaneous V-AV structures, which is the first objective of this Letter. Exactly how V-AV molecules transform into lattices (analogous to ionic colloidal crystals), and how they interact with (anti)fluxons introduced by external magnetic fields remain challenging questions for both theory and experiment, and this work yields critical insights in these areas.

In this Letter, we directly study V-AV structures in a Pb superconducting film deposited on a square array of magnetic dots with perpendicular magnetization (see Fig. 1), in an applied *homogeneous* magnetic field. Superconductor-ferromagnet hybrid systems can be broadly divided into two classes - those where magnetic nanostructures with *weak* moments are used as pinning sites to enhance the superconducting critical current by suppressing flux line motion [7], and those with *strong* moments which lead to the spontaneous formation of V-AV pairs. The latter have been found to enhance the critical temperature of the film at finite magnetic field through field compensation effects [8]. While such considerations are valid near the superconductor-normal phase boundary, where screening can be neglected ($j_c \approx 0$), the situation deep within the superconducting state is qualitatively different owing to the requirement for magnetic flux to be quantized. Here a simple picture of field cancelation is no longer applicable and a microscopic picture

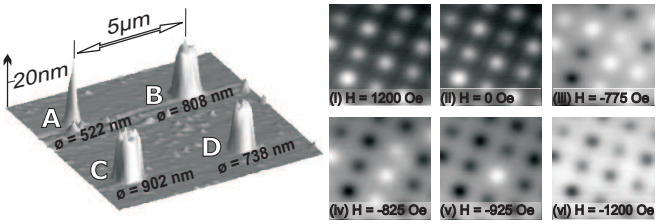

FIG. 1: AFM image of the magnetic disk array (left) and (i)-(vi) SHPM images of magnetization reversal (scan range is $\sim 17\mu$m $\times$ 17μm at 20K). The grayscale of images (i) and (ii) spans 2.66G and 2.63G respectively (see text).

of the formation of spontaneous V-AV pairs is essential along with an understanding of annihilation and trapping processes. This is a regime where, to date, very few experimental studies have been made (c.f. [9]).

To address the important outstanding issues in the low-temperature regime, we have performed high spatial resolution scanning Hall probe microscopy (SHPM) [10] on hybrid samples deep inside the superconducting state ($0.67 < T/T_c < 1$). The samples investigated consisted of a 1.5mm × 1.5mm array of ferromagnetic disks covered with a type II superconducting Pb film. The disks were formed in a $[Co(0.5nm)/Pt(1nm)]_{12}$ multilayer film sputtered on a Si/SO_2 substrate with uniaxial perpendicular magnetic anisotropy. They were patterned by electron beam lithography and reactive ion etching through an evaporated Al etch mask. Four different diameter circular disks with different magnetic moments have been patterned on the corners of a $5\mu m \times 5\mu m$ square cell which was repeated periodically in a square lattice, allowing the behavior of dots with different spontaneous V-AV numbers to be compared in the same sample. Design diameters of 522nm (dot A), 738nm (D), 808nm (B) and 902nm (C) were chosen, corresponding theoretically to 1, 3, 3 and 5 spontaneous V-AVs respectively [5]. Fig. 1 shows an atomic force micrograph of the unit-cell of the disk array. The unpatterned Co/Pt film was measured by the Magneto-Optical Kerr Effect (MOKE) at 300K and shown to have high remanence and a coercive field of $\sim$ 1000Oe. Fig. 1 shows SHPM images of magnetization reversal in the disks at $T = 20$K, indicating a range of coercive fields spanning 700-1000Oe and magnetic saturation above $\sim \pm 1000$Oe. Switching of the weakly coupled disks is largely uncorrelated, but once magnetized, disks of a given size exhibit very strong remanence at $H = 0$ and remain in a single domain state with highly uniform out-of-plane moments. The disks were coated with a 20nm Ge layer to suppress proximity effects and an 80nm Pb film deposited using dc magnetron sputtering followed by a 10nm Mo capping layer to prevent oxidation. Magnetization measurements on a single Pb film of the same thickness indicate that it is a type II superconductor with $T_c = 6.68$K, $\lambda_{eff}(5K) \approx 120$nm and $\xi(5K) \approx 50$nm. Finally the sample was also coated with 20nm Ge and 50nm Au to enhance the stability of the SHPM when in tunneling contact. Microscopy was performed in a 7T superconducting magnet at $T = 5$K with a $\sim 0.5\mu m$ spatial resolution GaAs/AlGaAs Hall sensor. Prior to imaging the Co/Pt dots were magnetized to saturation in an applied magnetic field of 3000Oe. An unwanted consequence of this was a small amount of trapped magnetic flux in our superconducting solenoid, with a remanent field ≈ -3.5Oe acting in the opposite direction to the (positive) dot magnetization. This 'background field' is estimated from a comparison between images and simulations (c.f. spontaneous V-AVs in Fig. 2 and "nulling" state in Fig. 4), and creates a constant offset to our applied field (H_a) axis in all cases. Defining the actual applied field as H_{eff} ($\cong H_a - 3.5$Oe) there are two noteworthy field conditions - the spontaneous V-AV state when $H_{eff} = 0$, and a "nulling" state (H_{null}) when all the spontaneous AVs have been exactly annihilated by externally added flux quanta. For $H_{eff} < 0$ we have excess 'free' AVs, for $0 < H_{eff} < H_{null}$ we have a gradual annihilation of spontaneous AVs, and for $H_{eff} > H_{null}$ we have free vortices.

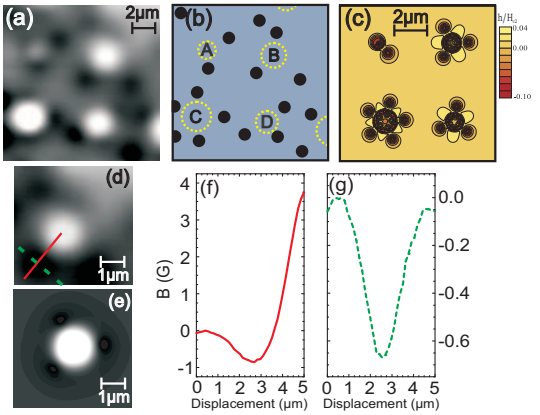

FIG. 2: (Color online) SHPM image of spontaneous V-AV configurations at $H_a = 3.5$Oe ($H_{eff} \approx 0$) and T=5K (a), and a schematic depiction of the AV locations (b) (dashed circles indicate the locations of magnetic disks). (c) Map of magnetic induction across theoretically predicted V-AV configurations. (d,e) Magnetic induction map across dot B, experiment (d) vs. theory (e). (f,g) Induction profiles across one AV along the lines indicated in (d).

Zero effective applied field. We focus first on spontaneous V-AV configurations at $H_{eff} \approx 0$. Fig. 2(a) shows the *first direct observation* of spontaneous V-AV shell structures. A strongly non-linear grayscale has been used to enhance identification of AVs. This can lead to apparent variations in AV intensity due to small variations in e.g. scan height, but does not influence our analysis which is based on identification of discrete fluxons. This SHPM image maps the full scan range of our microscope ($13\mu m \times 13\mu m$) and, in common with all other images presented here, was obtained after field-cooling. As expected, the (black) AVs clearly order in shell-like structures around the magnetic dots, while (white) vortices remain confined above the dots. Careful line-scan analysis allows one to determine the exact locations of AVs and these are sketched for clarity in Fig. 2(b). Fig. 2(c) illustrates the results of Ginzburg-Landau (GL) simulations for our exact sample geometry, obtained with coherence length $\xi(0) = 50$nm and uniform magnetization of the dots of $M = 750$G. Three dimensional calculations have also been performed to investigate the role of the topography introduced by the underlying disk array (for details of the approach we refer to Ref. [6]). The experimentally observed vorticity is in good agree-

ment with simulations, and broadly speaking increases with the magnetic moment of the disks (subject to flux quantization). Moreover, the agreement between experiment and theory is further apparent in Figs 2(d,e), which compare magnetic induction maps across magnet B. To highlight the structure of one of the bound AVs, Figs 2(f,g) show linescans of the induction profile in the two indicated orthogonal directions.

Negative effective applied fields. Fig. 3 illustrates the effect of introducing additional "free" AVs into the system by applying negative effective applied fields, $H_{eff} < 0$. Panel (a) shows the 'difference' image obtained after subtracting image 2 at $H_{eff} \approx -1$Oe from image 1 at $H_{eff} \approx 0$Oe. White spots in the difference image represent either unmatched AVs or 'annihilated' Vs in image 2. We see that two new AVs occupy interstitial sites between magnets while a third one *joins the AV shell* around dot D. The fourth remaining white spot cannot be associated with an AV, since it is located under the magnet itself. We conclude that, together with the adjacent black spot it *represents a V-AV pair* which has collapsed. In other words, the 738nm magnetic dot (D) which induced three V-AV pairs at $H_{eff} \approx 0$Oe, now generates only two in the sample at $H_{eff} \approx -1$Oe. In Figs. 3(b-e) we present a series of GL simulations to clarify this point. These illustrate Cooper-pair density plots obtained at $H_{eff} = 0$, -0.6, -1, and -1.8Oe respectively.

These figures clearly illustrate how the square symmetry of the underlying magnetic lattice imposes itself on the natural shell structure of the individual V-AV molecules. For example, in Fig. 3(c), with 3 added external AVs, one of the spontaneous AVs detaches from magnet B and joins the interstitial AV-lattice. Effectively, a spontaneous V-AV bond is *broken*, as the AV opts for the mutual interaction with other AVs rather than with its positive counterpart. In a reversal of this scenario for a larger number of external AVs (e.g. five in Fig. 3(d)), the excess AV, not needed in the interstitial lattice, approaches dot D, attracted by the positive core, and *joins the AV shell*. This does not, however, mean that the shell AV structure prevails over the square lattice. Quite the contrary, the new negatively charged V-AV molecule now acts as as a single component of the lattice. This is best illustrated in Fig. 3(e) (with nine external AVs), where all molecules have negative net charge (A:-2, B:-1, C:-1, D:-2).

Positive effective applied fields. The general behavior of the V-AV molecular crystal in a positive applied field is more intuitive, as it is mainly governed by the annihilation between AV shells and externally added vortices. With increasing applied field, each of the molecules progressively loses its negative "ions", and becomes positively charged. However, even after all AVs are annihilated, the vortex "charge" of individual magnetic dots keeps increasing due to the attraction between a magnet and a vortex when their moments are parallel [11]. This

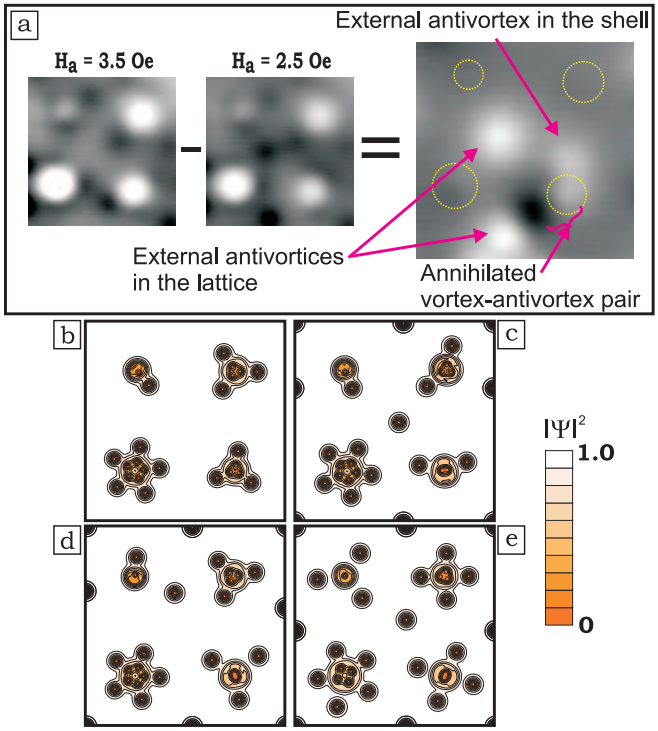

FIG. 3: (Color online) (a) SHPM images obtained at two different effective applied fields imaged at T=5K and their difference image (see text). (b-e) Cooper-pair density plots obtained theoretically for applied fields $H_{eff} = 0$, -0.6, -1, and -1.8Oe, respectively.

is emphasized in Fig. 4, where we show the number of experimentally measured off-site fluxons as a function of applied field, as well as the results of GL calculations. Both plots clearly show a "nulling" field ($H_a \approx 6$Oe), where we have *no free fluxons*. Importantly we find that this condition is met for a range of applied fields, i.e. ($\Delta H_a \geq 1$Oe). This 'locking' behavior, which arises due to the change in vortex occupation number of the magnetic disks, ensures the absence of any off-site fluxons, and consequently *enhances the critical current* of the sample. The asymmetry of our magnetic array cell is actually very beneficial here as it ensures pinning of *all* individual vortices added to the system and prevents their off-site ordering for non-commensurate numbers (so-called fractional matching).

Upon further increase of applied field, the non-uniform changes in on-site vortex occupation across the sample impact on off-site vortices. The potential landscape for the pinning of 'free' interstitial vortices becomes 'dynamic' since interactions with pinned vortex molecules relocate the energy minima as their charge changes. All the above effects are illustrated in the series of difference images, Figs. 4(i-iv), between the two indicated successive field-cooled states. Fig. 4(i) shows the annihilation of AVs (white spots) together with a decrease in the vortex occupation number of dot D (black spot). Fig. 4(ii) shows the change in occupation of the two lower

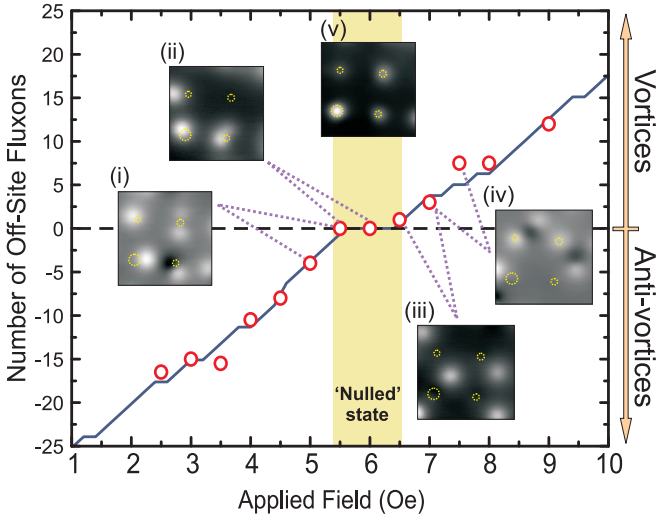

FIG. 4: (Color online) Number of experimentally observed free (anti)vortices vs. applied magnetic field (open dots) at T=5K. Solid line shows the predictions of GL theory (shifted by +4Oe on the field axis to simulate flux trapping in solenoid). (i)-(iv) Experimental SHPM difference images constructed between the indicated fields (see text). $\Delta H = 0.5$Oe corresponds to $\sim 3\phi_0$ per field-of-view on average. (v) Experimental SHPM image of the 'nulling' state ($H_a = 5.5$Oe).

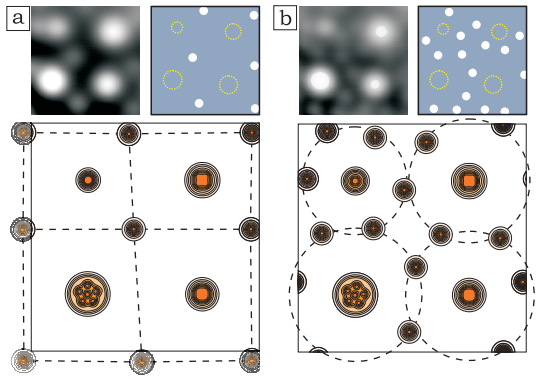

FIG. 5: (Color online) SHPM images at T=5K and corresponding Cooper-pair density plots illustrating formation of (a) an interstitial vortex lattice ($H_{eff} \approx 4.5$Oe), and (b) interstitial vortex shells for high vortex densities ($H_{eff} \approx 7.5$Oe).

disks near H_{null} (white spots), Fig. 4(iii) shows the crystallization of interstitial vortices (white spots), and Fig. 4(iv) shows the interaction-driven movement of vortices (adjacent pairs of black and white spots). Note that the off-center incorporation of new on-site vortices in Fig. 4(ii) is strongly indicative of a multi-vortex state above magnetic disks, in agreement with GL calculations.

Further proof that these phenomena arise due to competing interactions and not disorder is given in Fig. 5, which illustrates interstitial vortex structures at larger positive magnetic fields. At sufficiently large magnetic fields a square interstitial vortex lattice is recovered (Fig. 5(a)) mirroring conventional matching phenomena. However, the occupation number of the vortex "molecules" at each of the dots is different (A:2, B:5, C:6, D:4) which slightly distorts the lattice. The influence of multi-quanta vortices at the magnet sites becomes more evident at still higher vortex densities. The presence of four *different* repulsive potentials propagating radially from the corners of the square cell and strong interactions between interstitial vortices results in their arrangement in *shells* (c.f. Fig. 5(b)). Such an unusual ordering of vortices was never observed in the presence of uniform pinning. While AVs form shells around confined vortices due to their mutual attraction, uniquely and counter-intuitively, vortex shells are formed by repulsion. The same scenario applies generally to any system of interacting particles in a similar environment. Moreover, the complex V-AV interactions demonstrated in this Letter should also be reflected in two-component colloidal suspensions with oppositely charged particles, e.g. coated by charged polymers [12].

In conclusion, we have directly imaged spontaneous V-AV shell structures induced in superconducting films by the stray fields of magnetic arrays for the first time. We observe a variety of subtle phenomena which arise from competition between the n-fold rotational symmetry of the V-AV "molecules" and the translationally symmetric lattice of magnets. Our measurements agree with G-L calculations and give unique insights into the properties of ionic crystals based on the ordering of binary systems of particles, e.g. oppositely charged colloidal particles.

This work was supported by UK-EPSRC grant No. GR/D034264/1 and PhD studentship GR/P02707/01. M.V.M. is a Marie-Curie fellow at University of Bath.

* Also at: Departement Fysica, Universiteit Antwerpen, Groenenborgerlaan 171, B-2020 Antwerpen, Belgium
† Electronic address: s.bending@bath.ac.uk
‡ Current address: Diamond Light Source Ltd, Diamond House, Chilton, Didcot, Oxfordshire, OX11 0DE, UK

[1] C. Reichhardt and C.J. Olson, Phys. Rev. Lett. **88**, 248301 (2002); M. Brunner and C. Bechinger, Phys. Rev. Lett. **88**, 248302 (2002).
[2] P. Zeppenfeld *et al.*, Phys. Rev. Lett. **78**, 1504 (1997).
[3] K. Harada *et al.*, Science **274**, 1167 (1996).
[4] M.E. Leunissen, *et al.*, Nature (London) **437**, 235 (2005).
[5] M.V. Milošević and F.M. Peeters, Phys. Rev. B **68**, 024509 (2003).
[6] M.V. Milošević and F.M. Peeters, Phys. Rev. Lett. **93**, 124509 (2004); D.J. Priour, Jr. and H.A. Fertig, Phys. Rev. Lett. **93**, 057003 (2004).
[7] J.I. Martin *et al.*, Phys. Rev. Lett. **79**, 1929 (1997); D.J. Morgan *et al.*, Phys. Rev. Lett. **80**, 3614 (1998).
[8] S.A. Wolf, *et al.*, Phys. Rev. B **25**, 1990 (1982); H.W. Meul, *et al.*, Phys. Rev. Lett. **53**, 497 (1984); M. Lange, *et al.*, Phys. Rev. Lett. **90**, 197006 (2003).
[9] M. Lange *at al.*, Phys. Rev. B **72**, 052507 (2005).
[10] A. Oral *at al.*, Appl. Phys. Lett. **69**, 1324 (1996).

[11] S. Erdin, *et al.*, Phys. Rev. B **66**, 014414 (2002); M.V. Milošević and F.M. Peeters, Phys. Rev. B **68**, 094510 (2003); for review, see I. F. Lyuksyutov and V. L. Pokrovsky, Adv. Phys. **54**, 67 (2005).
[12] F. Caruso, *et al.*, Macromolecules **32**, 2317 (1999).